1.5 μm polarization entanglement generation based on birefringence in silicon wire waveguides

Ning Lv, Wei Zhang,* Yuan Guo, Qiang Zhou, Yidong Huang, and Jiangde Peng

Tsinghua National Laboratory for Information Science and Technology, State Key Laboratory on Integrated Optoelectronics, Department of Electronic Engineering, Tsinghua University, Beijing 100084, China

**Corresponding author: zwei@Tsinghua.edu.cn*

Received May 21, 2013; revised July 3, 2013; accepted July 3, 2013;
posted July 8, 2013 (Doc. ID 190841); published July 30, 2013

In this Letter, the 1.5 μm polarization entanglement generation is realized in a silicon wire waveguide utilizing its birefringence. In this scheme, two orthogonal polarized correlated states are generated by scalar processes of spontaneous four-wave mixing (SFWM) in the quasi-transverse electrical and quasi-transverse magnetic modes, respectively. Meanwhile, the vector processes of SFWM are suppressed by the group birefringence in the waveguide. The maximum polarization entangled state is generated by optimizing the pump polarization, which is demonstrated by the experiments of two-photon interference and polarization indistinguishability at one side. The fringe visibilities of two-photon interferences are $96.8 \pm 4.7\%$ and $86.0 \pm 3.7\%$ under two nonorthogonal polarization detection settings, respectively. This scheme provides a simple way to realize silicon integrated sources for 1.5 μm polarization entanglement generation.

OCIS codes: (270.5565) Quantum communications; (230.7370) Waveguides; (190.4380) Nonlinear optics, four-wave mixing; (190.4390) Nonlinear optics, integrated optics.
http://dx.doi.org/10.1364/OL.38.002873

Quantum light sources for 1.5 μm polarization entangled photon pair generation have important applications in quantum communication [1], quantum information processing [2], and quantum metrology [3,4]. Traditionally, polarization entangled photon pairs were generated by spontaneous parametric down conversion (SPDC) in nonlinear crystals [5,6], which has been widely used in researches of quantum optics. In recent years, to realize polarization entanglement generation in the optical communication band, several new schemes have been proposed and investigated, such as SPDC in periodically poled lithium niobate waveguides [7,8] and spontaneous four-wave mixing (SFWM) in optical fibers [9–14] and silicon wire waveguides (SWWs) [15]. Among them, the SFWM in SWWs attracts much attention. The third-order nonlinear coefficient of SWWs is about five orders of magnitude higher than silica fibers due to their ultrasmall modal areas and the high nonlinearity of silicon material [16]. On the other hand, since the spectrum of spontaneous Raman scattering in a SWW is quite narrow, the noise photons induced by it are easy to filter out. Hence, low-noise correlated/entangled photon pair generation can be realized at room temperature in SWWs. Furthermore, fabrication of SWWs is based on the techniques of silicon photonics, providing a potential to develop silicon integrated chips of quantum light sources.

However, the way to realize polarization entanglement generation in SWWs is not straightforward. It has been demonstrated that in an SWW, the intensity of SFWM in the quasi-transverse electrical mode (quasi-TE) is far higher than that in the quasi-transverse magnetic mode (quasi-TM) [17]. Hence, in the reported schemes, some special optical designs, such as a polarization-maintaining loop [15] or an on-chip polarization rotator at the midpoint of the SWW [18], are required to realize polarization entanglement generation utilizing the SFWM in TE mode only.

In this Letter, it is proposed that birefringence in SWWs provides a way to realize polarization entanglement generation in a simple straight SWW without any additional optical design. Similar with the SFWM in optical fibers [19], when pump light is injected into the SWW, two types of SFWM would be generated. One is the scalar process, in which two pump photons in the same waveguide mode (either quasi-TE or quasi-TM) are annihilated, while a pair of signal and idler photons are generated in the same mode. The other is the vector process, in which two annihilated pump photons are in different modes, the same for the generated signal and idler photons. If the vector processes are suppressed and the two scalar processes generate independently with equal intensity, the maximum polarization entangled state of $1/\sqrt{2}(|H_s\rangle|H_i\rangle + e^{i\varphi}|V_s\rangle|V_i\rangle)$ will be realized, where H and V denote the polarization directions of the generated photons corresponding to the two waveguide modes, namely the quasi-TE and quasi-TM modes, respectively; s and i denote the signal and idler photons, respectively. φ is the phase difference between the two orthogonal polarized correlated states generated in the two modes. It is worth noting that φ can be controlled by adjusting the polarization state of the pump light, which provides a way to realize bell states as [12] does.

Our previous work has demonstrated that the group birefringence can be utilized to suppress the vector processes in a piece of microstructured fiber [12]. Since the dispersions of the two modes in SWWs are quite different usually, it can be expected that this scheme may also be effective in the SWW. To demonstrate it, the photon pair generation rates of the scalar and vector processes in a typical SWW are calculated according to the theoretical methods proposed in [19]. The SWW is 3 mm in length. Its width and height are 500 and 220 nm, respectively, referred to the SWW sample used in the following experiment. Calculated by the finite element method, the nonlinear coefficients of its quasi-TE and quasi-TM modes are 176.8/W/m and 131.1/W/m, respectively. The dispersions of the quasi-TE and quasi-TM modes at 1.55 μm are −0.62 and 25.6 ps^2/m, respectively. The group birefringence $\Delta\beta_1$ is 2.2×10^{-9} s/m.

Figure 1 shows the calculation results when a linearly polarized pump light is injected into the SWW with a power of 200 mW and a polarization direction (denoted by θ) of 45° with respect to the H direction. Neglecting the coupling loss of the pump light, the pump powers in the quasi-TE and quasi-TM modes are assumed to be 100 mW for each. The photon pair generation rates for the scalar processes in the quasi-TE and quasi-TM modes are denoted by R_{HH} and R_{VV}, respectively. R_{HV} and R_{VH} are those for the two vector processes. Ω is the frequency detuning between the pump frequency and the frequencies of the signal/idler photons. In the calculation, the bandwidths of filters for the signal and idler photons are set as 30 GHz. It can be seen that all the SFWM processes generate photon pairs near the pump frequency. The bandwidth of R_{HH} is over 30 THz. The spectrum of R_{VV} is similar to that of R_{HH}; however, its spectral width is narrower and its intensity is weaker, which is due to the relatively larger dispersion and lower nonlinear coefficients of the quasi-TM mode. In the experiment, the coupling loss between the SWW and the lens fibers should be considered. The difference of R_{HH} and R_{VV} would be even larger, since usually the coupling loss for the quasi-TM mode is larger than that for the quasi-TE mode. On the other hand, the spectra of the two vector processes are far narrower than those of the two scalar processes because of the group birefringence in SWWs. The inset shows that the vector processes will be suppressed effectively if the frequency detuning Ω is higher than 0.4 THz.

The vector process suppression in SWWs can be utilized to realize polarization entanglement generation. To realize it, the photon pair generation rates in both quasi-TE and quasi-TM modes should be the same, which can be achieved by adjusting the input pump polarization direction θ to control the ratio of the pump powers in the two modes. Figure 2 shows the calculated total photon pair generation rates and the contributions of different processes of SFWM in the SWW under different pump polarization direction θ. Here, the input pump power is set as 200 mW, while the pump power in the quasi-TE and quasi-TM modes are assumed as 200 mW × cos θ and 200 mW × sin θ, respectively. The coupling loss of the pump light is not considered in the calculation. The frequency detuning Ω is set as 0.4 THz, which leads to an effective vector process suppression. Hence, the photon pairs are mainly generated by the two scalar processes in

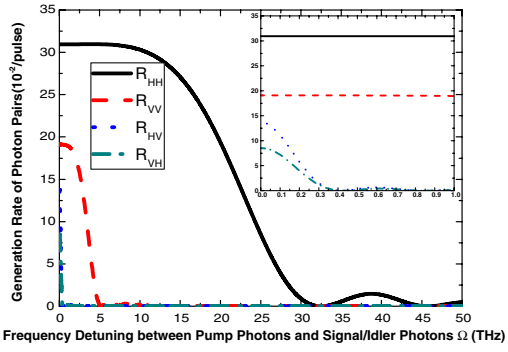

Fig. 1. Photon pairs generation rates spectra of the scalar and vector processes in an SWW under $\theta = 45°$. Inset: detail of the spectra between 0 and 1 THz.

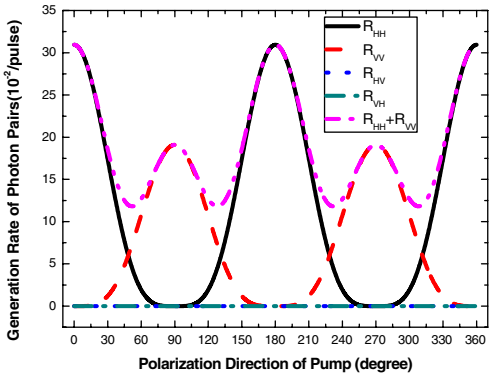

Fig. 2. Generation rate of photon pairs under different pump polarization directions with input pump peak power of 200 mW and Ω = 0.4 THz.

quasi-TE and quasi-TM modes. It can be seen that equal photon pair generation rates can be realized for the two scalar processes by adjusting the pump polarization direction to a proper angle, which is close to the angle for the minimum value of the total generation rates. In this case, the maximum polarization entanglement could be expected.

The experiment setup to demonstrate this scheme is shown in Fig. 3. A master oscillator power amplifier light source provides the pulsed pump light, in which the seed light pulses are generated from a directly modulated distributed feedback laser at 1.55 μm band and then amplified by an erbium-doped fiber amplifier. Its central wavelength, repetition rate, and pulse width are 1552.52 nm, 4 MHz, and 25 ps, respectively. The pump power is controlled by a variable optical attenuator (VOA). A rotatable half-wavelength plate (HWP) and a polarization controller (PC) are used to control the pump light polarization. The SWW sample (fabricated by Institute of Microelectronics IME, Singapore) used in the experiment is 3 mm in length. The width and height of its silicon core are 500 and 220 nm, respectively. Light is coupled into and out of the SWW by two lensed fibers. Inverse-taper structures with the tip width of 180 nm are designed at both ends of the SWW to improve the coupling efficiency [20]. The coupling between the lens fibers and SWW is realized by a high-precision manual-alignment system. The insertion loss of the SWW is −8.34 and −12.0 dB at 1.55 μm for the quasi-TE mode and quasi-TM modes, respectively. The large difference in the

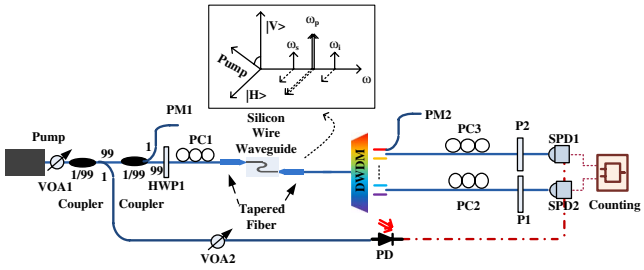

Fig. 3. Experimental setup. VOA, variable optical attenuator; P, polarizer; HWP, half-wavelength plate; PC, polarization controller; DWDM, dense wavelength division multiplexing; PD, photon detector; SPD, single-photon detector; PM, power monitor.

insertion losses of the two modes is mainly due to the difference of their coupling losses. Photon pairs will be generated when the pump light propagates through the SWW, then is directed to two single-photon detectors (SPD1 and SPD2, Id Quantique, id201) through a filtering system based on commercial dense wavelength division multiplexing (DWDM) components. The central wavelengths of the detected signal and idler photons are 1555.68 and 1549.30 nm, respectively. Hence, the frequency detuning Ω is about 0.4 THz in the experiment, ensuring that the vector processes are suppressed effectively as the theoretical analysis indicates. The spectral width of selected signal and idler photons are 0.25 and 0.27 nm, respectively. The insertion losses of the filtering system for the signal and idler photons are 1.69 and 1.09 dB, respectively. The SPDs operate in the gated Geiger mode with a detection window of 2.5 ns, triggered by the pump pulses from the 1:99 coupler through a VOA and a photon detector (PD). The detection efficiencies of the two SPDs are 8.0% and 8.7%, respectively, measured by attenuated pump pulses in the experiment preparation. Their dark count rates are measured as 6.8×10^{-5}/pulse and 5.9×10^{-5}/pulse, respectively. Two power monitors are used to monitor the power level of the input pump light (PM1) and the residual pump light through the DWDM (PM2).

To demonstrate polarization entanglement of the generated photon pairs, two polarization analyzers are inserted before the two SPDs. Each polarization analyzer consists of a PC and a polarizer. First, the polarization direction of the linearly polarized pump is set at the H direction by adjusting HWP1 and PC1, that is, $\theta = 0$, under which the pump light is coupled into the SWW and stimulates the quasi-TE mode. In this case, the correlated photon pairs are also generated in quasi-TE mode by the scalar process of SFWM and coupled out of the SWW with a polarization direction of H. By adjusting PC2 to realize the maximum signal side count, the signal-side polarization analyzer can be collimated to the H direction. Similarly, the idler-side polarization analyzer is also collimated to the H direction through PC3. After the collimation, the signal-side and idler-side polarization detecting directions (denoted byθ_s and θ_i, respectively, which are angles between the polarization detecting direction and the H direction at the two sides) can be adjusted by rotating P1 and P2, respectively, in the following experiment.

Then, polarization direction of the linearly polarized pump light is rotated by adjusting HWP1 to a certain angle θ, under which the smallest single-side count is measured. The calculation results in Fig. 1 have shown that the photon pair generation intensity in quasi-TE mode is far higher than that in quasi-TM mode under the same pump level, while the difference in coupling loss would farther enlarge the difference between the photon pair generation intensities in the two modes. Hence, to realize maximum entanglement, θ is close to 90° to couple more pump light into the quasi-TM mode to balance the photon pair generation rates in the two polarization directions.

The polarization entanglement of the generated photon pairs is demonstrated experimentally and shown in Fig. 4. Figure 4(a) is the experimental results of two-photon interference measurement, in which the coincidence

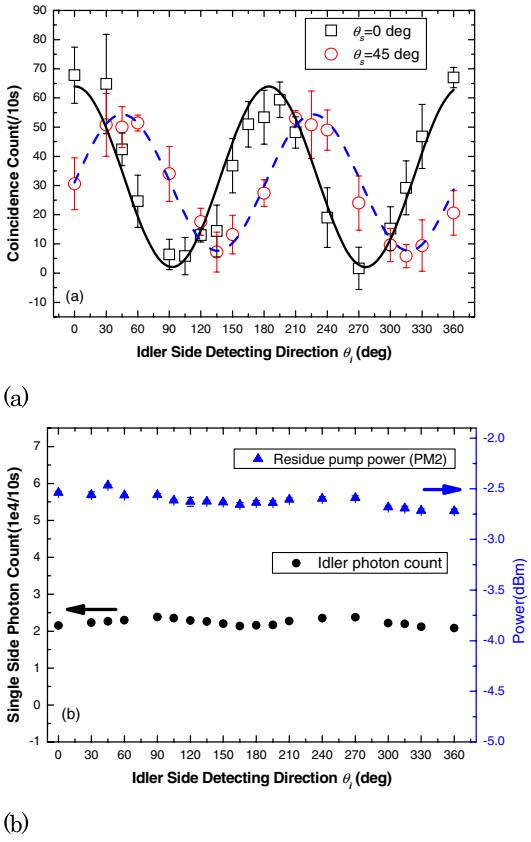

Fig. 4. Experiment results of polarization entanglement demonstration: (a) coincidence count under different θ_i and (b) idler-side photon count and residue pump power under different θ_i.

counts of the signal and idler photons are measured under different θ_i when θ_s is set as 0° and 45°, respectively. Each data point shown in Fig. 4(a) is an average of five measurements, and the counting time of each measurement is 10 s. The accidental coincidence count has been subtracted. Squares and circles are the results for $\theta_s = 0°$ and $\theta_s = 45°$, respectively. The solid and dashed curves are the fitted curves for the two cases, showing that the fringe visibilities of two-photon interference are $96.8 \pm 4.7\%$ for $\theta_s = 45°$ and $86.0 \pm 3.7\%$ for $\theta_s = 45°$. Better fringe visibility could be expected if the pump polarization is optimized carefully to control the phase difference φ to 0 or π.

It is worth noting that a relatively high pump level is used in the experiment due to the short waveguide length and low coupling efficiency of the SWW sample. Hence, the spontaneous Raman scattering in the fibers connecting the pump source and the SWW sample, including the pigtails of fiber devices and the lense fiber, cannot be neglected in the experiment, which may impact the fringe visibilities of the raw coincident counts (<70% under both polarization detection settings) significantly. Two ways could be expected to reduce this noise. One is reducing the pump level by improving the waveguide length and the coupling efficiency of the SWWs; the other is inserting an additional pump filter before the lensed fiber at the input end.

Figure 4(b) is the idler-side photon count (circles, with dark counts subtracted) under different θ_i. The residual

pump power (triangles, monitored by PM2 in Fig. 3) in the measurement is also plotted for comparison. It can be seen that the idler-side photon count is almost unchanged when θ_i varies. The small ripples on the curve are due to the variation of the pump light coupling to the SWW during the measurement process, which is indicated by the variation of the measured residual pump power. It indicates the polarization indistinguishability at the single side of the generated photon pairs. Combining the results shown in Figs. 4(a) and 4(b), it demonstrates that the generated photon pairs are in a polarization entangled state of $1/\sqrt{2}(|H_s\rangle|H_i\rangle + e^{i\varphi}|V_s\rangle|V_i\rangle)$.

In conclusion, this Letter proposes and demonstrates a simple scheme for 1.5 μm polarization entanglement generation in SWWs. The group birefringence in the SWW is utilized to suppress the vector processes of SFWM. By optimizing the pump polarization, two orthogonal polarized correlated states can be generated by two scalar processes of SFWM in quasi-TE and quasi-TM modes with equal intensity. It provides a way to realize a maximum polarization entangled state. The two-photon interference experiment shows that the fringe visibilities under two nonorthogonal polarization detection settings ($\theta_s = 0°$ and $\theta_s = 45°$) are $96.8 \pm 4.7\%$ and $86.0 \pm 3.7\%$, respectively. Meanwhile, polarization indistinguishability at the single side is also verified to demonstrate the polarization entanglement generation. This work provides a simple way to realize silicon integrated sources for 1.5 μm polarization entanglement generation.

This work is supported in part by the 973 Programs of China under Contract Nos. 2011CBA00303 and 2010CB327606, Tsinghua University Initiative Scientific Research Program, Basic Research Foundation of Tsinghua National Laboratory for Information Science and Technology (TNList), and China Postdoctoral Science Foundation.

References

1. N. Gisin, G. Ribordy, W. Tittel, and H. Zbinden, Rev. Mod. Phys. **74**, 145 (2002).
2. C. H. Bennett and S. J. Wiesner, Phys. Rev. Lett. **69**, 2881 (1992).
3. D. N. Klyshko, Sov. J. Quantum Electron. **7**, 591 (1977).
4. A. Migdall, Phys. Today **52**(1), 41 (1999).
5. P. G. Kwiat, K. Mattle, H. Weinfurter, A. Zeilinger, A. V. Sergienko, and Y. H. Shih, Phys. Rev. Lett. **75**, 4337 (1995).
6. C. Kurtsiefer, M. Oberparleiter, and H. Weinfurter, Phys. Rev. A **64**, 023802 (2001).
7. S. Tanzilli, H. De Riedmatten, W. Tittel, H. Zbinden, P. Baldi, M. De Micheli, D. B. Ostrowsky, and N. Gisin, Electron. Lett. **37**, 26 (2001).
8. H. Takesue, K. Inoue, O. Tadanaga, Y. Nishida, and M. Asobe, Opt. Lett. **30**, 293 (2005).
9. X.-Y. Li and P. Kumar, Phys. Rev. Lett. **94**, 53601 (2005).
10. M. Medic, J. B. Altepeter, M. A. Hall, M. Patel, and P. Kumar, Opt. Lett. **35**, 802 (2010).
11. H. Takesue and K. Inoue, Phys. Rev. A **70**, 31802 (2004).
12. Q. Zhou, W. Zhang, J. R. Cheng, Y. D. Huang, and J. Peng, Opt. Lett. **34**, 2706 (2009).
13. E. Meyer-Scott, V. Roy, J.-P. Bourgoin, B. L. Higgins, L. K. Shalm, and T. Jennewein, Opt. Express **21**, 6205 (2013).
14. Y. M. Sua, J. Malowicki, M. Hirano, and K. F. Lee, Opt. Lett. **38**, 73 (2013).
15. H. Takesue, H. Fukuda, T. Tsuchizawa, T. Watanabe, K. Yamada, Y. Tokura, and S. Itabashi, Opt. Express **16**, 5721 (2008).
16. H. Fukuda, K. Yamada, T. Shoji, M. Takahashi, T. Tsuchizawa, T. Watanabe, J. Takahashi, and S. Itabashi, Opt. Express **13**, 4629 (2005).
17. K. Harada, H. Takesue, H. Fukuda, T. Tsuchizawa, T. Watanabe, K. Yamada, Y. Tokura, and S. Itabashi, IEEE J. Select. Topics Quant. Electron. **16**, 325 (2010).
18. N. Matsuda, H. Le Jeannic, H. Fukuda, T. Tsuchizawa, W. J. Munro, K. Shimizu, K. Yamada, Y. Tokura, and H. Takesue, Sci. Rep. **2**, 817 (2012).
19. E. Brainis, Phys. Rev. A **79**, 023840 (2009).
20. V. R. Almeida, R. R. Panepucci, and M. Lipson, Opt. Lett. **28**, 1302 (2003).